Parity-time-symmetry–enhanced sideband generation in an optomechanical system

Ling-Yan He*

School of Science, Beijing University of Posts and Telecommunications, Beijing 100876, China
and John A. Paulson School of Engineering and Applied Sciences, Harvard University, Cambridge, Massachusetts 02138, USA

(Received 23 October 2018; published 22 March 2019)

Optical high-order sideband generation, creating new frequencies with equal spectral separation, has developed potential applications in optical communication and metrology. Here, we investigate the generation of optomechanically induced high-order optical sideband spectra in an optical parity-time ($\mathcal{PT}$) -symmetric system. The system consists of an active optical mode, a passive optical mode, and a mechanical mode, where the mechanical mode is optomechanically coupled with the passive optical mode. Based on numerical analysis, the $\mathcal{PT}$-symmetric system enhances sideband spectra in both amplitude and number of sidebands. With certain parameters, forty sidebands head up on both sides of the control field near the exceptional point. The capability to generate optical high-order sidebands and control light propagation in micro- and nanomechanical systems may open up a promising perspective for complex integrated $\mathcal{PT}$ devices.

DOI: 10.1103/PhysRevA.99.033843

I. INTRODUCTION

"Physics would be dull and life most unfulfilling if all physical phenomena around us were linear. Fortunately, we are living in a nonlinear world, where nonlinearity provides excitement in physics." This is remarked in the famous nonlinear optics book [1]. Generating new photons at different frequencies, as a consequence of nonlinear processes, has found its place ranging from fundamental studies on light-matter interactions to applications in optical communication and metrology. Optical high-order sideband generation provides coherent outputs related to its input light through a nonlinear manner [2–7]. Without certain enhancements, such small nonlinearity is challenging to observe and hinders potential applications in quantum information processing and communication. Optical microcavities, providing extremely high-quality factors with small mode volumes [8–10], have emerged as an essential platform to enhance nonlinear optical phenomena. Cavity optomechanics (COM) [11–17] provides unprecedented opportunities to study the interaction between optical fields and mechanical oscillations, such as optomechanically induced transparency (OMIT) [18–23], slow light [24], and optical sideband generation [25,26]. Importantly, optomechanically induced nonlinearity does not depend on the nonlinearity of material and thus enables efficient optical sideband generation for most dielectric materials.

On the other hand, the parity-time ($\mathcal{PT}$) symmetry [27,28] has been studied theoretically and experimentally in both optical and optomechanical microresonators. Manipulating such $\mathcal{PT}$-symmetric structures has enabled novel applications such as nonreciprocal light transmission [29–34] or sensors [35–38], loss-induced lasing revival [39], and optical parametric amplification [40]. Recent advances in $\mathcal{PT}$-symmetric optics reveal unique effects including phonon lasing [41,42], symmetry-breaking chaos [43], OMIT in microresonators [44–46], and high-order exceptional point optomechanics [47].

There is a pioneering work which investigates the nonlinear OMIT with gain and loss, and they find the transmission of the second-order sideband pulse can be significantly enhanced in the vicinity of gain-loss balance [25]. In this work, we systematically explore the parameter space for second-order sideband generation in a hybrid COM system benefiting from $\mathcal{PT}$ symmetry. Also, we further investigate the optomechanically induced generation of optical high order sidebands in a $\mathcal{PT}$-symmetric system and show the transition of higher-order sideband generation from passive-passive to active-passive regime in the weak intensity limit and saturable gain regime, respectively. The system is composed of two coupled microcavities. One is lossy (passive cavity) and the other is associated with optical gain (active cavity). We show that (i) the efficiency of the second-order sideband generation in the proposed active-passive cavities can be enhanced by over forty times and (ii) the number of sidebands could be substantially extended.

This paper is organized as follows. In Sec. II, we present our model of a nonlinear $\mathcal{PT}$-assisted active-passive compound COM system for optical sideband generation. In Sec. III, we analyze optical second-order sideband generation on various parameters, including the gain-to-loss ratio and photon-tunneling strength between two cavities. In Sec. IV, we present the amplitude and number of optical high-order sidebands could be substantially enhanced by choosing proper parameters. Finally, we summarize and outlook.

II. THEORETICAL MODEL

Our system is composed of two microtoroid cavities with two optical whispering gallery modes and one mechanical mode (Fig. 1). The active cavity can be fabricated by doping the erbium ions, which provides gain κ to compensate

*lyhe@seas.harvard.edu

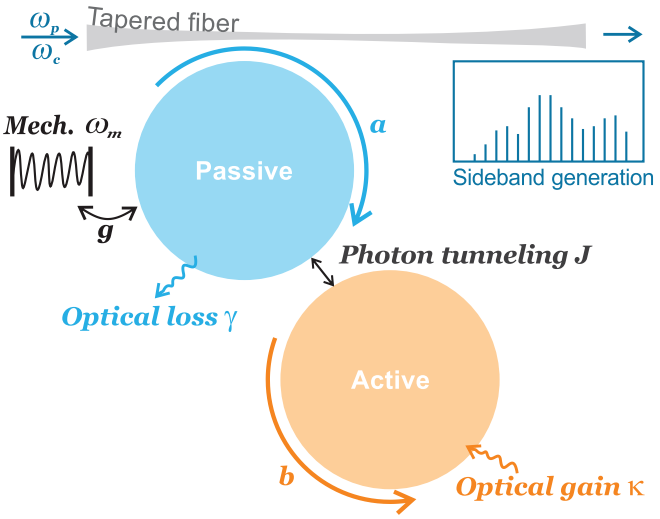

FIG. 1. Schematic diagram of high-order sideband generation process in an active-passive COM structure. The left cavity mode is coherently pumped by a continuous-wave control field and a probe field. The mechanical mode is localized in the passive cavity and characterized by a resonant frequency ω_m, damping rate Γ_m, an effective mass m, and optomechanical coupling constant g. The other cavity with optical gain is active, while the optical nonlinearity is omitted. Two cavities are directly coupled by the coherent photon tunneling strength J. The optical excitation is achieved by a tapered fiber coupled to the passive cavity with the coupling rate κ_e. The cavity output can be monitored by using an optical spectrum analyzer. The inset shows the transmission characteristics of high-order optical sidebands.

the optical loss γ in the passive cavity when driven by a pump laser in the 980 nm or 1460 nm bands [32]. The optical mode is pumped by a bichromatic laser field $S_{\rm in}(t) = (E_c e^{-i\omega_c t} + E_p e^{-i\omega_p t})$, with the amplitudes $E_c = \sqrt{P_c/\hbar\omega_c}$ and $E_p = \sqrt{P_p/\hbar\omega_p}$, respectively, where P_c and P_p denote the powers of the control and probe lasers. ω_c (ω_p) is the frequency of the control (probe) field. $S_{\rm in}$ ($S_{\rm out}$) represents the input (output) field propagating in the waveguide.

The Hamiltonian of this composite system is given by

$$\begin{aligned} H =& \hbar\Delta(a^\dagger a + b^\dagger b) + \frac{p^2}{2m} + \frac{1}{2}m\omega_m^2 x^2 \\ &- \hbar g a^\dagger a x - \hbar J(a^\dagger b + a b^\dagger) \\ &+ i\hbar\sqrt{\kappa_e}[(E_c + E_p e^{-i\Omega t})a^\dagger - \text{H.c.}], \end{aligned} \tag{1}$$

where a (b) and $a^\dagger$ ($b^\dagger$) represent the bosonic annihilation and creation operators of the passive (active) cavity mode. ω_a and ω_b are the resonance frequencies of the two cavities. For the $\mathcal{PT}$-symmetric structure, we assume the same resonant frequency for both cavities, i.e., $\omega_a = \omega_b = \omega_0$. x and p denote the mechanical position and momentum operators. The detunings between the cavity field, the control laser, and the probe laser are represented by $\Delta = \omega_0 - \omega_c$, $\Delta_p = \omega_p - \omega_0$, and $\Omega = \omega_p - \omega_c = \Delta_p + \Delta$, respectively. We choose $\Delta = \omega_m$, resulting in $\Delta_p = \omega_p - \omega_c = \Omega - \omega_m$.

Based on the Hamiltonian and introducing the dissipation terms by using the Markov approximation, the Heisenberg-Langevin equations of motion for the $\mathcal{PT}$-symmetric system can be written as

$$\begin{aligned} \dot{a} &= (-i\Delta + igx - \gamma)a + iJb + \sqrt{\kappa_e}(E_c + E_p e^{-i\Omega t}), \\ \dot{b} &= (-i\Delta + \kappa)b + iJa, \\ \dot{x} &= p/m, \\ \dot{p} &= -m\omega_m^2 x + \hbar g a^\dagger a - \Gamma_m p. \end{aligned} \tag{2}$$

Here the evolution of the optical field is considered in a rotating frame at the frequency ω_c of the optical excitation signal. Note that $\gamma > 0$, $\kappa > 0$ in Eq. (2) corresponds to an active-passive compound COM system, while $\gamma > 0$, $\kappa < 0$ corresponds to a passive-passive system.

Equations (2) are nonlinear and coupled equations due to the parametric coupling between optical and mechanical modes. It should be noted that the above equation cannot be solved exactly, as the steady-state response is composed of an infinite number of different frequencies. However, in weak probe field limit, the dynamics around the steady-state solution can be analyzed perturbatively. The solution of Eq. (2) can be written as $a = a_s + \delta a$, $b = b_s + \delta b$, $x = x_s + \delta x$, where a_s, b_s, x_s are the steady-state solutions when $E_p = 0$, δa, δb, δx are the fluctuations and displacement of the cavity field driven by the probe field, respectively. Substituting the above perturbation expansion ansatz into Eq. (2), the steady-state solution is obtained as

$$\begin{aligned} x_s &= \frac{\hbar g}{m\omega_m^2}|a_s{}^2|, \\ a_s &= \frac{\sqrt{\kappa_e}E_c(i\Delta - \kappa)}{(i\Delta - \kappa)(\gamma + i\Delta - igx_s) + J^2}, \\ b_s &= \frac{i\sqrt{\kappa_e}JE_c}{(i\Delta - \kappa)(\gamma + i\Delta - igx_s) + J^2}. \end{aligned} \tag{3}$$

The perturbation expansion terms are given by

$$\begin{aligned} \delta a &= A_1^- e^{-i\Omega t} + A_1^+ e^{i\Omega t} + A_2^- e^{-2i\Omega t} + A_2^+ e^{2i\Omega t}, \\ \delta b &= B_1^- e^{-i\Omega t} + B_1^+ e^{i\Omega t} + B_2^- e^{-2i\Omega t} + B_2^+ e^{2i\Omega t}, \\ \delta x &= X_1 e^{-i\Omega t} + X_1^* e^{i\Omega t} + X_2 e^{-2i\Omega t} + X_2^* e^{2i\Omega t}, \end{aligned} \tag{4}$$

where A_n^- and A_n^+ are the coefficients of nth-order higher and lower sidebands.

The parametric frequency conversion results from the nonlinearity [corresponding to the terms $-ig\delta x\delta a$ and $(\hbar g/m)\delta a^*\delta a$] in the optomechanical system. When the control and probe fields are incident upon the optomechanical cavity, the two-tone driving energy is transferred to the sidebands with a series of new frequencies $\omega_N = \omega_c \pm N\Omega$, where N is the number of the sidebands. $N = 0$ corresponds to the control field ω_c, $N = 1$ corresponds to the probe field (i.e., the anti-Stokes field), and $N = -1$ is the first lower sideband (i.e., the Stokes field), and so on. The amplitudes of the

second-order sidebands are given by

$$
\begin{aligned}
A_1^- &= \frac{\left[\left(\omega_m^2 - \Omega^2 - i\Omega\Gamma_m\right)G_2 m + ig^2 n_1 \mu_2\right]\mu_1 E_p\sqrt{\kappa_e}}{\left(\omega_m^2 - \Omega^2 - i\Omega\Gamma_m\right)G_1 G_2 m - ig^2 n_1 (G_2\mu_1 - G_1\mu_2)},\\
A_1^+ &= \frac{ig^2 {a_s}^2 {\mu_1}^* {\mu_2}^*}{\left(\omega_m^2 - \Omega^2 + i\Omega\Gamma_m\right){G_1}^* {G_2}^* m + ig^2 n_1 ({G_2}^* {\mu_1}^* - {G_1}^* {\mu_2}^*)},\\
A_2^- &= \frac{g^3 {a_s}^2 {A_1^+}^* X_1 \mu_3\mu_4 - ig^2 a_s {A_1^+}^* A_1^- \mu_3 G_4 + igA_1^- X_1\mu_3\left[G_4 m\left(\omega_m^2 - 4\Omega^2 - 2i\Omega\Gamma_m\right) + ig^2 n_1\mu_4\right]}{\left(\omega_m^2 - 4\Omega^2 - 2i\Omega\Gamma_m\right)G_3 G_4 m + ig^2 n_1 (G_3\mu_4 - G_4\mu_3)},\\
X_1 &= \frac{g{a_s}^* G_2 E_p \mu_1}{\left(\omega_m^2 - \Omega^2 - i\Omega\Gamma_m\right)G_1 G_2 m - ig^2 n_1 (G_2\mu_1 - G_1\mu_2)},
\end{aligned}
\tag{5}
$$

with

$$
\begin{aligned}
n_1 &= |a_s|^2,\\
\mu_1 &= -\kappa - i\Omega + i\Delta,\ \mu_2 = -\kappa - i\Omega - i\Delta,\\
\mu_3 &= -\kappa - 2i\Omega + i\Delta,\ \mu_4 = -\kappa - 2i\Omega - i\Delta,\\
G_1 &= (i\Delta + \gamma - igx_s - i\Omega)\mu_1 + J^2,\\
G_2 &= (-i\Delta + \gamma - igx_s - i\Omega)\mu_2 + J^2,\\
G_3 &= (i\Delta + \gamma - igx_s - 2i\Omega)\mu_3 + J^2,\\
G_4 &= (-i\Delta + \gamma - igx_s - 2i\Omega)\mu_4 + J^2.
\end{aligned}
\tag{6}
$$

Using the input-output relation $S_{\text{out}} = S_{\text{in}} - \sqrt{\kappa_e}a$, the output field is

$$
S_{\text{out}} = c_0 + c_1^- e^{-i\Omega t} + c_1^+ e^{i\Omega t} + c_2^- e^{-2i\Omega t} + c_2^+ e^{2i\Omega t}, \tag{7}
$$

where the coefficients are $c_0 = E_c - \sqrt{\kappa_e}a_s$, $c_1^- = E_p - \sqrt{\kappa_e}A_1^-$, $c_1^+ = -\sqrt{\kappa_e}A_1^+$, $c_2^- = -\sqrt{\kappa_e}A_2^-$, and $c_2^+ = -\sqrt{\kappa_e}A_2^+$, respectively. c_0 corresponds to the control field with frequency ω_c, c_1^- is the coefficient of the first-order lower sideband, and the term c_2^- corresponds to the second-order lower sideband generation process, in which the output field with frequency $\omega_c - 2\Omega$ is produced. And the term c_2^+ is of the second-order upper sideband. The efficiency of optical second-order sideband generation is given by

$$
\eta = |-\sqrt{\kappa_e}A_2^-/E_p|. \tag{8}
$$

For simplicity, we discuss the lower sideband in the following.

To respect $\mathcal{PT}$ symmetry, $J - (\gamma + \kappa_e + \kappa)/4$ should be greater than zero, which equaling to zero is the exceptional point (EP) [32]. In our work, we assume that $\kappa_e = 2\gamma$ for simplicity unless stated otherwise. For instance, when $J = \gamma$ indicating unchanged photon-tunneling strength J between two cavities, we require $0 < \kappa/\gamma < 1$. When $\kappa = \gamma$ indicating balance between gain and loss, we require $J > \gamma$.

III. ENHANCEMENT OF HIGH-ORDER SIDEBAND SPECTRA GENERATION AND EFFECTIVE TUNING

In this section, we discuss the dependence of second-order sideband generation on the gain-to-loss ratio κ/γ and the photon-tunneling strength J in two distinct systems: passive-passive and active-passive. We compute the efficiency of the optical second-order sideband η, with experimentally accessible parameter values [21], which are summarized in Table I.

A. Dependence of the second-order sideband on the gain-to-loss ratio

Figure 2(a) depicts the efficiency η of the second-order sideband generation as a function of the probe detuning Δ_p in both non-$\mathcal{PT}$-symmetric and $\mathcal{PT}$-symmetric regimes. The transmission spectra of the second-order sideband exhibit two sideband peaks. Clearly, for active-passive compound COM system ($\kappa/\gamma > 0$), the generation efficiency is maximized when the gain and loss are balanced, i.e., $\kappa/\gamma = 1$. Interestingly, the optimum condition happens in the vicinity of EP. Also, the smallest linewidth of η is achieved at the EP. Note that the values of spectral peaks are considerably higher compared to that of the passive-passive compound COM system ($\kappa = -\gamma$). By optimizing the gain-to-loss ratio κ/γ, η rockets up by over forty times from 1.05% (passive-passive) to 46% (active-passive).

The intuitive explanation follows: under the condition of the fixed photon-tunneling strength $J = \gamma$, the system transits from $\mathcal{PT}$-symmetric to the broken-$\mathcal{PT}$-symmetric phase when κ/γ goes over one. In the region $0 < \kappa/\gamma < 1$, the gain compensates the loss in the passive cavity and leads to the sideband amplification of the transmission spectrum. Increasing the gain above the EP pushes the system into the broken-$\mathcal{PT}$-symmetric phase, and the optical supermodes become spontaneously localized in either the active or the passive cavity [32]. Thus there is a localized net loss at the optomechanical cavity. In this way, the field intensity in the passive cavity significantly decreases as well as the transmission rate of the second-order sideband.

Figure 2(b) illustrates the maximum transmission efficiency of the second-order sideband as a function of κ/γ. For a passive-passive hybrid COM system, the transmission

TABLE I. List of parameters used in the numerical calculations.

Parameter	Value
ω_m	$2\pi \times 51.8$ MHz
ω_0	$2\pi \times 193$ THz
g	$2\pi \times 12$ GHz/nm
m	2×10^{-11} kg
Γ_m	$2\pi \times 41$ kHz
J	$2\pi \times 15$ MHz
γ	$2\pi \times 15$ MHZ

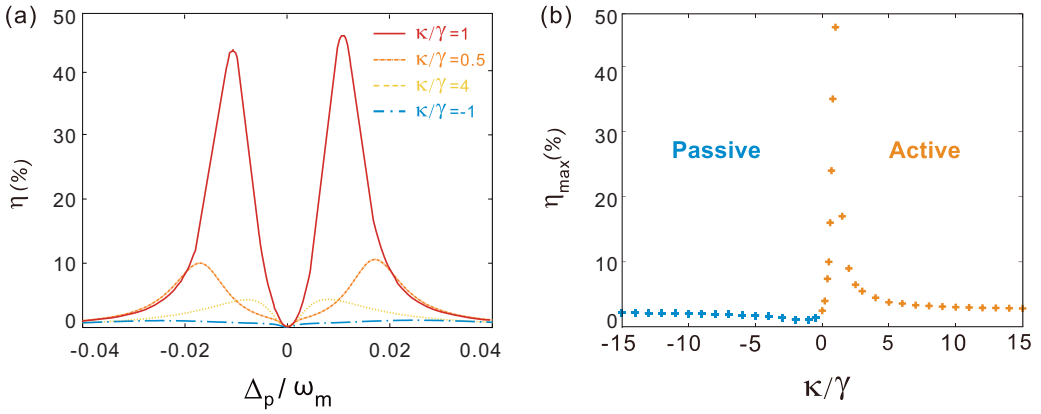

FIG. 2. (a) Efficiency rate η of the probe light versus the optical detuning $\Delta_p = \omega_p - \omega_0$, for different values of the gain-to-loss ratio. The optical tunneling rate is fixed as $J/\gamma = 1$. (b) Maximum transmission rate of the second-order sideband generation η of the probe field versus the gain-to-loss ratio κ/γ with $\Delta_p = \omega_m$. Other parameters are as in Table I.

peak is insensitive to the gain-to-loss ratio [see the blue + in Fig. 2(b)]. Instead, for an active-passive COM system, the two sideband peaks increase sharply when the gain in the active cavity increases [see the orange + in Fig. 2(b)]. The transmission peaks of sidebands are maximized at $\kappa/\gamma = 1$. Afterwards, the sideband peaks are greatly suppressed. These results are consistent with the above discussions, shown in Fig. 2(a).

B. Dependence of the second-order sideband spectra on the photon-tunneling rate

Here, we discuss the influence of the photon-tunneling rate J on the efficiency of the second-order sideband generation η (Fig. 3). For a small value of coupling strength $J = 0.2\gamma$, the spectrum of η, in the passive-passive compound COM system, shows two sideband peaks reaching 2.3%. As for the active-passive compound COM system, the second-order sideband features two higher sideband peaks. When we raise the photon-tunneling rate to $J = 2\gamma$, in the passive-passive double cavity system, the peaks shift towards both sides and the value of η is reduced to 0.8%. In this case, the double-cavity coupling becomes more competitive; the generation of the second-order sideband tends to be suppressed by the strong photon-tunneling effect. On the other hand, for the active-passive double cavity system, the system transits from broken-$\mathcal{PT}$-symmetric phase to $\mathcal{PT}$-symmetric phase. The spectrum of η displays two slightly lower sideband peaks with wider linewidth. We find that the efficiency of the second-order sideband generation is higher in the $\mathcal{PT}$-symmetric regime, whether in the strong or weak photon-tunneling coupling condition.

For further insight, the variation of the maximum value of η with photon-tunneling strength J/γ for the passive-passive and the $\mathcal{PT}$-symmetric double-cavity system is depicted in Fig. 4. The second-order sideband generation of the passive-passive COM system decreases exponentially in the range $0 < J/\gamma < 2$. However, the behavior of η becomes substantially different when the gain is introduced into the cavity. η_{max} increases with the increase of J and reaches its maximum value when $J/\gamma = 1$; then it experiences a sharp reduction. In contrast to passive-passive double-cavity system, the values of η in active-passive double-cavity system are overall enhanced. This implies that $\mathcal{PT}$-symmetric structure can amplify the second-order sideband signal effectively by simply changing the distance between two cavities. The coupling strength decreases exponentially with increasing distance between two cavities, thus changing the number and intensity of the output

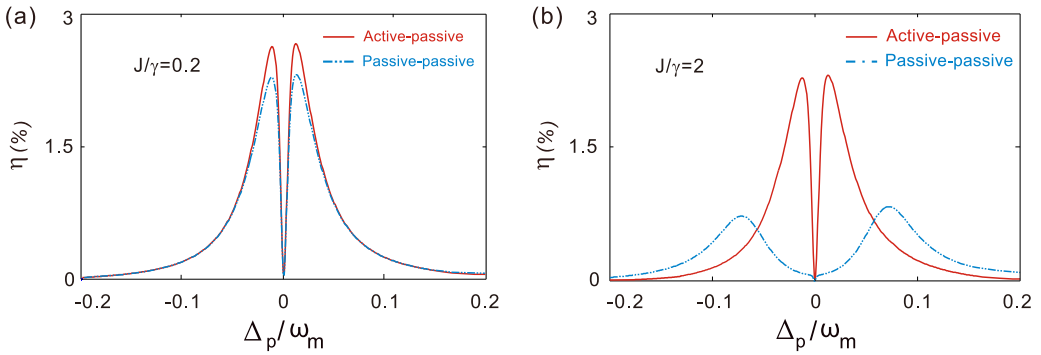

FIG. 3. Calculation result of η as a function of the detuning Δ_p under two different values of the coupling strength J for the passive-passive compound COM system (i.e., $\kappa/\gamma = -1$) and the active-passive compound COM system (i.e., $\kappa/\gamma = 1$). We use the coupling strength $J/\gamma = 0.2$ and $J/\gamma = 2$.

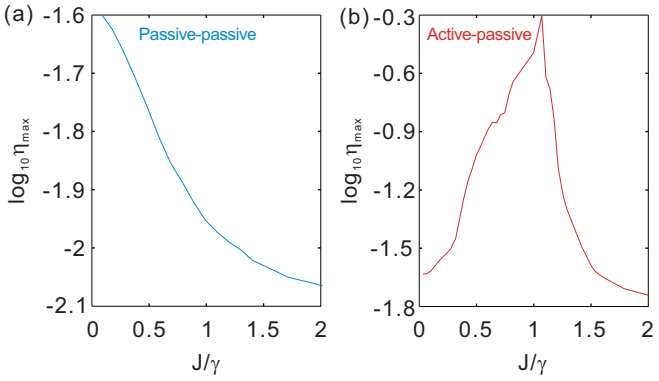

FIG. 4. Maximum value of η in logarithmic scale changes with the photon-tunneling rate J for (a) the passive-passive and (b) the active-passive compound COM system with $\Delta_p = \omega_m$.

spectra. The photon tunneling strength in our proposal can be realized in experiments.

IV. GENERATION OF OPTICAL HIGH-ORDER SIDEBAND SPECTRA IN $\mathcal{PT}$-SYMMETRIC REGIME

Finally, we numerically discuss the higher-order sideband generation with a tunable gain-to-loss ratio. Two conditions of optical gain are discussed: (i) in weak intensity limit, where the optical gain, κ, is considered as a constant, and (ii) for high intensities, the saturation of the gain should be included.

A. Linear gain condition

In the linear regime, the higher-order sidebands generation enhances from the passive-passive to active-passive regime (Fig. 5). For two lossy cavities [lower region in Fig. 5(a)], i.e., $\kappa/\gamma < 0$, there are only a few sidebands generated. The brightest line at the center corresponds to the control field, and the first-order lower and upper sidebands are the Stokes and anti-Stokes fields, respectively. The spectral spacing between observed sidebands equals $\Omega = \omega_p - \omega_c$ as expected. The highest order we observe in the two lossy cavities is the sixth order. For example, when $\kappa/\gamma = -8$, the highest order above 10^{-3} we observe is only three [Fig. 5(b)]. As one cavity becomes less lossy, the amplitude and number of the higher-order sidebands increases slightly. When one cavity experiences net gain, i.e., $\kappa/\gamma > 0$, the system enters the active-passive regime [upper region in Fig. 5(a)]. The intensity of higher-order sidebands increases; for example, the sixth-order sideband increases to $10^{-2.3}$. More than 10 sidebands on each side are generated [Fig. 5(c)]. The amplitude of the 10th-order sideband is about 10^{-3}. As the gain-to-loss ratio increases, there is a gradual increase in both amplitude and number of the sidebands generated when approaching the PT-phase transition.

Two features attribute to the enhancement of sideband generation. (i) Due to gain to loss balance, the supermodes of the system are almost lossless. In the strong-coupling regime, the supermodes are distributed evenly across the cavities [48]; therefore, the absorption can be compensated by the gain and the effective damping rate of the system decreases. The energy flows from the gain cavity to the lossy one in a highly efficient way. (ii) The effective interaction strength between the optical modes and the mechanical mode is significantly enhanced, as discussed in Ref. [48].

The enhancement of the higher-order sideband generation in the $\mathcal{PT}$-symmetric compound COM system originates from the square root of complex energy in the parameter space [49,50]. The $\mathcal{PT}$ symmetry in all the above discussions validates only in the linear limit, i.e., the gain in the active cavity is independent upon the intensities. When the gain-to-loss approaches EP, the intensity of the sidebands would be infinity, similar to the results in Refs. [34,51]. This is due to the spectral singularities, which spoil the completeness of eigenvectors. The transmission tends to grow infinitely when gain and loss tends to be balanced, which has been previously investigated by Mostafazadeh [52,53] because of the linearity of the system.

B. Nonlinear gain-saturated condition

In this section, we discuss the high-order sideband generation in the nonlinear regime. The gain will saturate at high input probe power; further increasing the power may decrease the effective gain in the system, especially when there is a high-Q factor cavity in the system. The saturable gain

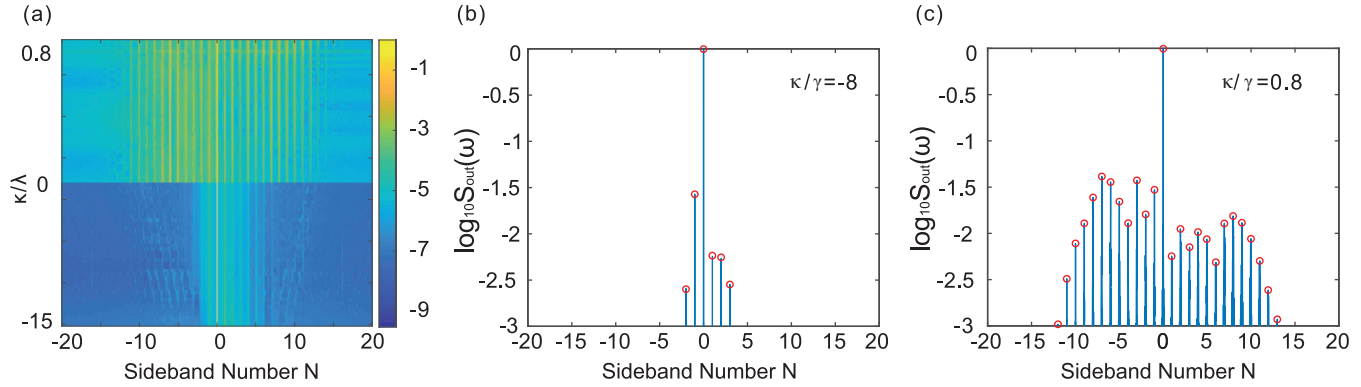

FIG. 5. (a) Transmitted output (in logarithmic scale) of the generated higher-order sidebands as a function of the gain-to-loss ration κ/γ and sideband number N. Panels (b) and (c) are the the passive-passive (i.e., $\kappa/\gamma = -8$) and active-passive compound COM system (i.e., $\kappa/\gamma = 0.8$), respectively. The other system parameters are in Table I.

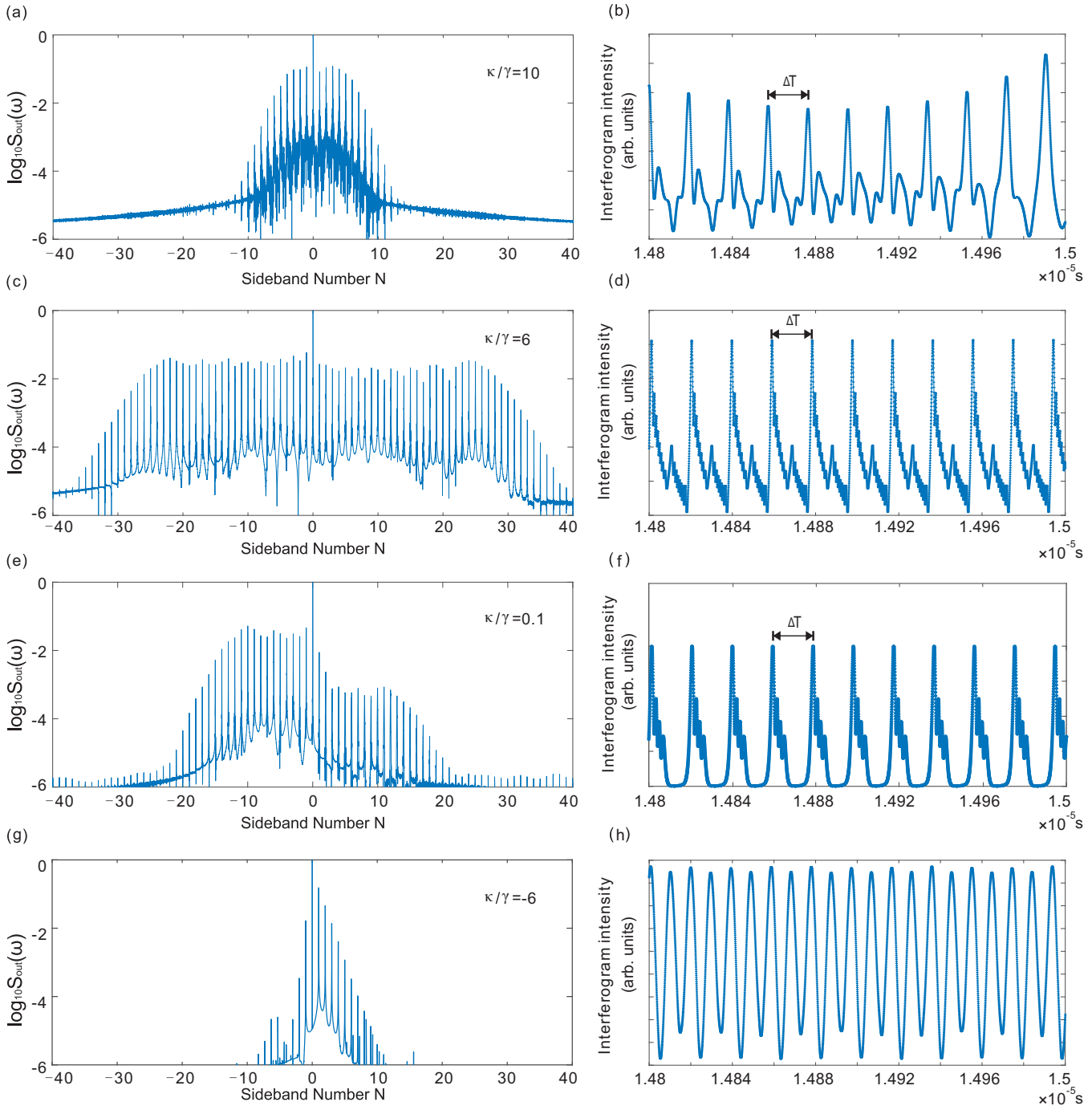

FIG. 6. Spectra and real-time interferogram intensity of transmitted output in (a),(b) the broken $\mathcal{PT}$ symmetric phase, (c),(d) EP, (e),(f) the $\mathcal{PT}$ symmetric phase, and (g),(h) the passive-passive regime. At EP, $J = (\gamma + \kappa_e + \kappa)/4$. The parameters are $J = 2\gamma$, $\kappa_e = \kappa$, and $\Delta T = 1/\omega_m = 1.93e^{-8}$ s.

$\kappa' = \kappa_0 \frac{1}{1+|\frac{b}{b_{\rm sat}}|^2}$, where κ_0 is the gain at $b = 0$ and $b_{\rm sat}$ corresponds to the gain saturation threshold. Under this condition, we numerically solve the reformulated Heisenberg-Langevin equations of motion and then performing fast Fourier transform. We obtain the transmitted output of the generated higher-order sidebands as shown in Fig. 6. In the time domain, a continuous wave is observed in two lossy cavities [Fig. 6(h)], while pulses are observed when cavity gain is introduced [Figs. 6(b), 6(d) and 6(f)]. The period of pulses corresponds to the mechanical mode, i.e., $\Delta T = 2\pi/\omega_m = 1.93 \times 10^{-8}$ s. The passive-passive system only generates a narrow-bandwidth spectrum with 10 sidebands above the intensity of 10^{-6} [Fig. 6(g)]. The active-passive system extends the sideband spectrum to higher order; the broadest sideband spectrum is achieved near EP [Fig. 6(c)]. Forty sidebands head up on both sides of the control field near EP. Tuning the gain away from the EP will narrow the spectra [Figs. 6(a) and 6(e)]. Counterintuitively, a stronger gain does not necessarily lead to

a broader spectrum in the $\mathcal{PT}$-symmetry system. As the gain in the active cavity becomes larger, the system enters the broken $\mathcal{PT}$-symmetric phase; one supermode vanishes because of the absorption, while the other experiences amplification [54]. The spacing between sidebands is determined by the mechanical mode, instead of the free spectral range of the optical mode; therefore, our system is free from the optical dispersion.

V. SUMMARY

In summary, we theoretically investigated the generation of second-order and higher-order sidebands in a $\mathcal{PT}$-symmetric compound COM system. The higher-order sideband spectra can be greatly enhanced in the $\mathcal{PT}$-symmetric system. This work paves the way to observation of optical nonlinearities with low power and proposes an approach for strong high-order sideband generation. Furthermore, there are potential applications in optical frequency comb generation and optical communication based on the optomechanical platform [55], and promising perspectives for integrated optoelectronic $\mathcal{PT}$ devices. The repetition rate of optomechanical frequency combs is the mechanical resonant frequency, ranging from a few megahertz to tens of gigahertz [56]. For such a low repetition rate, an optical Kerr frequency comb requires a centimeter-sized optical cavity, while optomechanical combs do not rely on an optical free spectral range.

ACKNOWLEDGMENTS

I thank L. Shao, Y. Hu, Prof. C. Wang, and C. Cao for valuable discussions. This work is supported by the Beijing University of Posts and Telecommunications Excellent Ph.D. Students Foundation No. CX2016209.

[1] Y.-R. Shen, *The Principles of Nonlinear Optics* (Wiley-Interscience, New York, 1984), p. 575.
[2] T. Carmon and K. J. Vahala, Nat. Phys. **3**, 430 (2007).
[3] H. Xiong, L.-G. Si, A.-S. Zheng, X. Yang, and Y. Wu, Phys. Rev. A **86**, 013815 (2012).
[4] J. Li, J. Li, Q. Xiao, and Y. Wu, Phys. Rev. A **93**, 063814 (2016).
[5] H. Suzuki, E. Brown, and R. Sterling, Phys. Rev. A **92**, 033823 (2015).
[6] C. Cao, S.-C. Mi, Y.-P. Gao, L.-Y. He, D. Yang, T.-J. Wang, R. Zhang, and C. Wang, Sci. Rep. **6**, 22920 (2016).
[7] H. Xiong, L.-G. Si, X.-Y. Lü, and Y. Wu, Opt. Express **24**, 5773 (2016).
[8] S. M. Spillane, T. J. Kippenberg, K. J. Vahala, K. W. Goh, E. Wilcut, and H. J. Kimble, Phys. Rev. A **71**, 013817 (2005).
[9] Y. Louyer, D. Meschede, and A. Rauschenbeutel, Phys. Rev. A **72**, 031801 (2005).
[10] K. J. Vahala, Nature (London) **424**, 839 (2003).
[11] J.-Q. Liao, H. K. Cheung, and C. K. Law, Phys. Rev. A **85**, 025803 (2012).
[12] X.-W. Xu, H. Wang, J. Zhang, and Y.-X. Liu, Phys. Rev. A **88**, 063819 (2013).
[13] M. Ludwig, A. H. Safavi-Naeini, O. Painter, and F. Marquardt, Phys. Rev. Lett. **109**, 063601 (2012).
[14] X.-Y. Lü, W.-M. Zhang, S. Ashhab, Y. Wu, and F. Nori, Sci. Rep. **3**, 2943 (2013).
[15] M.-A. Lemonde, N. Didier, and A. A. Clerk, Phys. Rev. Lett. **111**, 053602 (2013).
[16] D. W. Schönleber, A. Eisfeld, and R. El-Ganainy, New J. Phys. **18**, 045014 (2016).
[17] I. S. Grudinin, H. Lee, O. Painter, and K. J. Vahala, Phys. Rev. Lett. **104**, 083901 (2010).
[18] A. H. Safavi-Naeini, T. M. Alegre, J. Chan, M. Eichenfield, M. Winger, Q. Lin, J. T. Hill, D. E. Chang, and O. Painter, Nature (London) **472**, 69 (2011).
[19] G. S. Agarwal and S. Huang, Phys. Rev. A **81**, 041803(R) (2010).
[20] A. Kronwald and F. Marquardt, Phys. Rev. Lett. **111**, 133601 (2013).
[21] S. Weis, R. Rivière, S. Deléglise, E. Gavartin, O. Arcizet, A. Schliesser, and T. J. Kippenberg, Science **330**, 1520 (2010).
[22] C. Dong, V. Fiore, M. C. Kuzyk, and H. Wang, Science **338**, 1609 (2012).
[23] H. Lü, Y. Jiang, Y.-Z. Wang, and H. Jing, Photon. Res. **5**, 367 (2017).
[24] D. Chang, A. H. Safavi-Naeini, M. Hafezi, and O. Painter, New J. Phys. **13**, 023003 (2011).
[25] Y. Jiao, H. Lü, J. Qian, Y. Li, and H. Jing, New J. Phys. **18**, 083034 (2016).
[26] Y.-F. Jiao, T.-X. Lu, and H. Jing, Phys. Rev. A **97**, 013843 (2018).
[27] C. E. Rüter, K. G. Makris, R. El-Ganainy, D. N. Christodoulides, M. Segev, and D. Kip, Nat. Phys. **6**, 192 (2010).
[28] C. M. Bender, Rep. Prog. Phys. **70**, 947 (2007).
[29] H. Ramezani, T. Kottos, R. El-Ganainy, and D. N. Christodoulides, Phys. Rev. A **82**, 043803 (2010).
[30] L. Feng, M. Ayache, J. Huang, Y.-L. Xu, M.-H. Lu, Y.-F. Chen, Y. Fainman, and A. Scherer, Science **333**, 729 (2011).
[31] Z. Lin, H. Ramezani, T. Eichelkraut, T. Kottos, H. Cao, and D. N. Christodoulides, Phys. Rev. Lett. **106**, 213901 (2011).
[32] B. Peng, Ş. K. Özdemir, F. Lei, F. Monifi, M. Gianfreda, G. L. Long, S. Fan, F. Nori, C. M. Bender, and L. Yang, Nat. Phys. **10**, 394 (2014).
[33] X. Liu, S. Dutta Gupta, and G. S. Agarwal, Phys. Rev. A **89**, 013824 (2014).
[34] L. Chang, X. Jiang, S. Hua, C. Yang, J. Wen, L. Jiang, G. Li, G. Wang, and M. Xiao, Nat. Photon. **8**, 524 (2014).
[35] W. Chen, Ş. K. Özdemir, G. Zhao, J. Wiersig, and L. Yang, Nature (London) **548**, 192 (2017).
[36] J. Wiersig, Phys. Rev. Lett. **112**, 203901 (2014).
[37] H. Hodaei, A. U. Hassan, S. Wittek, H. Garcia-Gracia, R. El-Ganainy, D. N. Christodoulides, and M. Khajavikhan, Nature (London) **548**, 187 (2017).
[38] R. Fleury, D. Sounas, and A. Alu, Nat. Commun. **6**, 5905 (2015).
[39] B. Peng, Ş. Özdemir, S. Rotter, H. Yilmaz, M. Liertzer, F. Monifi, C. Bender, F. Nori, and L. Yang, Science **346**, 328 (2014).
[40] R. El-Ganainy, J. I. Dadap, and R. M. Osgood, Opt. Lett. **40**, 5086 (2015).

[41] H. Jing, S. K. Özdemir, X.-Y. Lü, J. Zhang, L. Yang, and F. Nori, Phys. Rev. Lett. **113**, 053604 (2014).
[42] H. Lü, S. K. Özdemir, L.-M. Kuang, F. Nori, and H. Jing, Phys. Rev. Appl. **8**, 044020 (2017).
[43] X.-Y. Lü, H. Jing, J.-Y. Ma, and Y. Wu, Phys. Rev. Lett. **114**, 253601 (2015).
[44] H. Jing, Ş. K. Özdemir, Z. Geng, J. Zhang, X.-Y. Lü, B. Peng, L. Yang, and F. Nori, Sci. Rep. **5**, 9663 (2015).
[45] H. Lü, C. Wang, L. Yang, and H. Jing, Phys. Rev. Appl. **10**, 014006 (2018).
[46] H. Zhang, F. Saif, Y. Jiao, and H. Jing, Opt. Express **26**, 25199 (2018).
[47] H. Jing, Ş. Özdemir, H. Lü, and F. Nori, Sci. Rep. **7**, 3386 (2017).
[48] J. Zhang, B. Peng, Ş. K. Özdemir, K. Pichler, D. O. Krimer, G. Zhao, F. Nori, Y.-X. Liu, S. Rotter, and L. Yang, Nat. Photon. **12**, 479 (2018).
[49] W. Heiss, J. Phys. A **45**, 444016 (2012).
[50] E. Hernández, A. Jáuregui, and A. Mondragón, J. Phys. A **39**, 10087 (2006).
[51] Z.-P. Liu, J. Zhang, Ş. K. Özdemir, B. Peng, H. Jing, X.-Y. Lü, C.-W. Li, L. Yang, F. Nori, and Y.-X. Liu, Phys. Rev. Lett. **117**, 110802 (2016).
[52] A. Mostafazadeh, Phys. Rev. Lett. **102**, 220402 (2009).
[53] A. Mostafazadeh and H. Mehri-Dehnavi, J. Phys. A **42**, 125303 (2009).
[54] J. Wen, X. Jiang, L. Jiang, and M. Xiao, J. Phys. B **51**, 222001 (2018).
[55] M.-A. Miri, G. D'Aguanno, and A. Alù, New J. Phys. **20**, 043013 (2018).
[56] M. J. Burek, J. D. Cohen, S. M. Meenehan, N. El-Sawah, C. Chia, T. Ruelle, S. Meesala, J. Rochman, H. A. Atikian, M. Markham, D. J. Twitchen, M. D. Lukin, O. Painter, and M. Lončar, Optica **3**, 1404 (2016).